# Aqueous Zirconium Complexes for Gelling Polymers. A Combined X-ray Absorption Spectroscopy and Quantum Mechanical Study

**Jérôme Rose,*,† Theodorus J. M. De Bruin,‡ Guy Chauveteau,‡ René Tabary,‡ Jean-Louis Hazemann,§ Olivier Proux,§ Aziz Omari,|| Hervé Toulhoat,‡ and Jean-Yves Bottero†**

*CEREGE, UMR 6635 CNRS/Université Aix-Marseille III, IFR PMSE 112, Europole Méditerranéen de l'Arbois, BP80, 13545 Aix en Provence Cedex 4, France, IFP, BP311, 92506 Rueil-Malmaison, France, Laboratoire de Cristallographie CNRS 38042 Grenoble Cedex 9, France, and MASTER-ENSCPB, 16 av. de Peberland, 33607 Pessac Cedex, France*

*Received: October 2, 2002; In Final Form: January 8, 2003*

The reinforcement of regulations concerning environment protection in most countries is a strong incentive to use "green" cross-linkers for sol−gel processes. Among them, water soluble zirconium complexes seem attractive for various applications in the surface coatings , oil production, sol stabilization, and agriculture industries. Moreover, recent works demonstrated that a zirconium lactate−polyacrylate solution leads to the formation of size controlled microgels under shear flow. The speciation of zirconium, both in aqueous solutions (zirconium lactate) and in polymer gels (a terpolymer of acrylamide), was determined by combining X-ray absorption spectroscopy (XAS) and quantum mechanical calculations using density functional theory. XAS experiments were performed at the Zr−K-edge at the European Synchrotron Radiation Facility by using fluorescence detection in order to get results down to very low concentrations (37 ppm). The X-ray absorption near edge structure (XANES) results show that Zr is mainly surrounded by eight oxygens in the first coordination sphere, forming a dodecahedron. The analysis of extended X-ray absorption fine structure (EXAFS) spectra combined with quantum mechanical calculations results indicates that, in the concentrated zirconium lactate solutions (53300 ppm), which was found to be stable over years, the zirconium complexes are dimers ($(Zr)_2(lactate)_6$) surrounded by six bidentate lactate ligands. As zirconium lactate concentration is decreased, the dimers condense first in cyclic tetramers ($Zr_4$ $(lactate)_X$) and then in larger oligomers by tetramer association. In polyacrylamide microgels ([Zr] = 74 and 148 ppm) the Zr species remains dimers when gelation is completed at pH = 6, whereas tetramers are also observed at pH = 7. The XAS spectra were characterized by a very high signal-to-noise ratio, making possible to observe the gelation, i.e., the exchange of lactate by acrylate ligands.

## 1. Introduction

The control of cross-linking kinetics in sol−gel systems is the key point in several industrial processes such as ceramic manufacturing, thin film formation, surface coatings, and permeability control to enhance oil recovery. Two types of sol−gel processes are of industrial importance. The first is based on the hydrolysis and condensation of metal alkoxides leading to the formation of oxopolymers which form strong gels and is extremely important for ceramic synthesis. The second type is the gelling of organic polymers containing hydroxyl or carboxyl groups by using organo-metallic cross-linkers consisting of di-, tri-, or tetra-valent cations complexed by organic ligands. The main advantage of polymer gels is that gel strength can be reduced as desired. For example, in the oil industry, very weak gels are needed to reduce water production without affecting oil recovery.

Until now, in most industrial applications, chromium is still frequently used as a cross-linker for gelling organic polymers. However, the toxicity of $Cr^{6+}$ restricts its use in many situations, creating a strong incentive to use "green" cross-linkers such as zirconium complexes. Recently, several authors have studied the gelling mechanisms responsible for the cross-linking of polyacrylamide solutions by using zirconium citrate[1,2] or lactate.[3,4,5] In addition to it being a green product, the use of zirconium lactate or citrate makes it possible to control cross-linking kinetics, which determine the final structure and homogeneity of the gels. This kinetic control aspect is particularly crucial when the objective is to obtain size-controlled microgels.[3,4,5] The original method to prepare such microgels consists of cross-linking, under steady shear, a homogeneous solution containing both a polymer and the cross-linker zirconium lactate. This method is very different from the microgel formation in emulsion polymerization.[6] In the case of oil production, these microgels are expected to control water mobility at long distances from the wells to improve sweep efficiency and reduce selectively permeability to water for water production control. Moreover, microgels appear as quasi-ideal candidates to develop permanent or temporary water or pollutant barrier in soil. Then, microgels appear to be very promising to improve several environmental processes that require the control of both water mobility and soil permeability such as treatment of contaminated sites (soils, groundwater, etc.).

* Author to whom correspondence should be addressed. Tel: (33) 442 971 529, fax: (33) 442 971 559, e-mail: rose@cerege.fr.
† Université Aix-Marseille III.
‡ IFP.
§ Laboratoire de Cristallographie CNRS.
|| MASTER-ENSCPB.

10.1021/jp027114c CCC: $25.00 
Published on Web 03/07/2003

However, the process optimization requires the identification of the cross-linking species and the conditions under which these species remain stable over long periods of time. This characterization is the aim of the present study and was achieved by combining X-ray absorption spectroscopy (XAS) with quantum mechanical calculations.

## 2. Background: Zirconium Speciation in Solution

In aqueous solutions in the absence of strong ligands, the hydrolysis of Zr species as pH increases is now well-documented. In acidic conditions, zirconium remains under monomeric form and is surrounded by eight water molecules, thus forming a dodecahedron.[7] As other tetravalent cations in aqueous solution, zirconium hydrolyzes spontaneously and forms $[Zr(OH)(OH_2)_7]^{3+}$ monomeric complexes. If the pH increases, the former complex can evolve to form the $[Zr(OH)_2(OH_2)_6]^{2+}$ monomer. The condensation of the latter complex through olation reaction (1) leads to the polymerization of the monomers and the formation of a cyclic tetramer.[7,8]

$$4\,[Zr(OH)_2(OH_2)_6]^{2+} \rightarrow [Zr_4(OH)_8(OH_2)_{16}]^{8+} + 8H_2O \qquad (1)$$

In terms of structure, each of the four zirconium dodecahedra in the tetramer shares two edges with its two zirconium neighbors.[9] This cyclic structure has been identified with different techniques such as ultracentrifugation,[10] wide and small angle scattering.[11,12,13] Further hydrolysis of the $[Zr_4(OH)_8(OH_2)_{16}]^{8+}$ complex increases the number of $OH^-$ groups around the zirconium cations and leads to the formation of Zr $\langle^{OH}_{OH}\rangle$ Zr linkages between the tetramers. However, the final product depends on the hydrolysis conditions, namely the rate of pH increase. A fast hydrolysis leads to the formation of a zirconium gel without spatial arrangement or order at any scale of observation.[8,14,15] By contrast, a slow hydrolysis favors more ordered structures such as $Zr(OH)_4$. This type of polymerization occurs in the case of nitrate, chloride, or perchlorate zirconium salts, because these anions are easily replaced by the stronger $OH^-$ ligands. When strong ligands are present during hydrolysis (phosphate, sulfate, carboxylate, chelate, etc.), the polymerization route is different[15] and leads to the formation of mixed zirconium−anion compounds.

In alcoholic solvents and in the presence of organic ligands, much of the information found in the literature concerns the synthesis of ceramics via sol−gel processes. Indeed, the process commonly used consists of initiating the sol−gel reactions by adding water in an alcohol solution containing zirconium alkoxides ($Zr(OR)_n$). This technique allows a good control of the polymerization reaction leading to ceramics with well-controlled properties. The main result is that, in alcoholic solvent, the association of free solvent molecules and zirconium complexes hinders the zirconium polymerization. For example, in the case of zirconium butoxide and propoxide in their parent solvent, Peter et al.[16] proposed solvated Zr-dimers or trimers or mixtures of both as possible structures. Helmerich et al.[17] also confirmed the presence of small zirconium species (dimers and trimers) by using XAS. When a ligand stronger than butoxide such as acetylacetone (acac) is added to the solution, three complexes have been identified: $Zr_2(OR)_{10}$ dimer, $Zr_2(OR)_{10}(acac)_2$ dimer, and $Zr(acac)_4$ (zirconium-(acetylacetone)$_4$) monomer.[8,17,18] The proportion of $Zr_2(OR)_{10}(acac)_2$ and $Zr(acac)_4$ versus $Zr_2(OR)_{10}$ changes, depending on the concentration of acetylacetone. When acetylacetone is in excess, only the monomer $Zr(acac)_4$ is found in solution.[19] For other ligands such as acetic acid, zirconium dimer species still exist, even in excess of ligand.[17] Thus, in the presence of a strong ligand and under conditions which prevent hydrolysis (i.e. low pH and excess of ligands), the monomeric complex $Zr(ligand)_4$ represents the major species.[19] A polymerization of such complexes leading to the formation of the Zr dimer, $Zr_2(ligand)_6$, was observed by different authors[8,16,18,19] when the pH was slightly increased, but the general trend is that strong ligands have the property to hinder or to block the polymerization of zirconium.

As far as we know, there is no information in the literature concerning the zirconium speciation in aqueous system containing lactate and/or acrylate. However, literature data show that EXAFS (extended X-ray absorption fine structures), which is a part of the XAS spectra, has been found to be extremely well-suited to the analysis of the nature of species in solution and the evolution, during the first hydrolysis stages, for metal cations such as iron,[20,21,22] chromium,[23,24] gallium,[25] titanium,[26] and zirconium[17,19,27]. As suggested by this literature survey, we performed XAS experiments, analyzed the data, and compared the results with that of quantum mechanical calculations (density functional calculations = DFT) in order to increase the reliability of our conclusions concerning zirconium speciation.

## 3. Experimental Section

**3.1. Zirconium Lactate Stock Solution.** The concentrated zirconium lactate solution used was provided by Benchmark Research and Technology Inc. The Zr weight concentration was 53300 ppm, and the initial pH was 7.50. The [lactate]/[Zr] molar ratio, called *X*, was 3.

**3.2. Polymer Solutions.** The polymer used for gelling experiments was a high molecular weight (MW $\approx 5 \times 10^6$ g · mol$^{-1}$) terpolymer provided by Floerger, containing 96% acrylamide groups, 2% sulfonates to prevent syneresis, and 2% acrylates to ensure cross-linking with zirconium. This polymer is referred to as HSPAM (hydrolyzed sulfonate polyacrylamide) in the text.

**3.3. Diluted Zirconium Lactate Solutions.** Two series of experiments were performed to investigate the effect of both dilution and aging on zirconium speciation in lactate solution. In the first series, the effect of the dilution factor on Zr speciation was determined after 20 min of aging in a 20 g/l NaCl solution and pH = 6. The final Zr weight concentrations were 1035, 592, 148, and 37 ppm. After aging, the solution was directly analyzed.

In the second series, the effects of time were investigated on zirconium lactate solutions at [Zr] = 74 ppm and pH = 6 or 5 in 20 g/l NaCl solutions. The pH and temperature (20 °C) were carefully kept constant during and after the dilution experiments. The solutions were introduced in a sample holder and frozen in liquid nitrogen to stop the evolution of the Zr polymerization after 20, 120, and 360 min. During XAS measurements, samples were maintained in a frozen state using a cryostat.

**3.4. Preparation of HSPAM Gels.** For obtaining HSPAM gels, the zirconium lactate solutions were prepared at 74 ppm in a 20 g/l NaCl solution, allowed to stand for 20 min, and then mixed in a 50/50 volume ratio with a 4 g/l HSPAM solution at the same pH. In a first series of experiments, aimed at investigating the pH effect, two gels formed at pH = 6 and 7 were analyzed by XAS after 5 days. For this set of samples, the dilution of zirconium lactate solution was performed in excess of lactate, i.e., $X$ = [lactate]/[Zr] = 6.

For the second series of experiments, aimed at investigating aging, the speciation was determined 40, 120, and 540 min after the mixing between zirconium lactate and HSPAM solutions at pH = 6. Gels in formation were put in a sample holder and

**TABLE 1: Structural Parameters Derived from EXAFS Analysis of the Crystalline Reference Compounds and Compared with XRD Data**

| sample name | filter window (Å) | atomic pair | $R_{EXAFS}$ (Å) | $R_{XRD}$ (Å) | $\sigma$ (Å) | $N_{EXAFS}$ | $N_{XRD}$ | $\Delta E_0$(eV) | Q[a] |
|---|---|---|---|---|---|---|---|---|---|
| $Zr(C_6H_7O_2)_4$ | 1.27−2.10 | Zr−O | 2.12 | *2.08*[39] | 0.051 | 2.0 | *2.0*[33] | 3.0 | 0.012 |
| Zr−acac | | Zr−O | 2.22 | *2.19*[39] | 0.071 | 6.0 | *6.0*[33] | 3.0 | |
| | 2.53−3.65 | Zr−C | 3.24 | *3.20*[39] | 0.065 | 7.3 | *8.0*[33] | 18.0 | 0.041 |
| | | Zr−C | 3.68 | *3.60*[39] | 0.055 | 4.8 | *4.0*[33] | 18.0 | |
| $ZrOCl_2 \cdot 8H_2O$ | 1.22−2.35 | Zr−O | 2.12 | *2.12*[9] | 0.079 | 4.85 | *3.0*[9] | 0.0 | 0.016 |
| | | Zr−O | 2.30 | *2.30*[9] | 0.071 | 2.65 | *5.0*[9] | 0.0 | |
| | 2.77−3.67 | Zr−Zr | 3.57 | *3.56*[9] | 0.055 | 1.8 | *2.0*[9] | −2.5 | 0.022 |
| $Zr(C_4H_9O)_4$ | 2.33−3.58 | $Zr-C_1$ | 3.03 | *3.03*[16] | 0.035 | 2.3 | *2.3*[16] | 18 | 0.043 |
| (Zr-butoxide) | | $Zr-C_2$ | 3.18 | *3.50*[16] | 0.061 | 5.0 | *5.0*[16] | 18 | |
| | | Zr−Zr | 3.56 | *3.51*[16] | 0.059 | 0.7 | *1.0*[16] | −0.4 | |
| zircone | 1.22−2.35 | Zr−O | 2.15 | *2.13*[40] | 0.083 | 4.0 | *4.0*[34] | 0.0 | 0.058 |
| $ZrSiO_4$ | | Zr−O | 2.26 | *2.26*[40] | 0.113 | 4.0 | *4.0*[34] | 0.0 | |

[a] $Q = \Sigma[([(k^3\chi_{calculated} - k^3\chi_{experimental})]^2)/((k^3\chi_{experimental})^2)]$.

frozen in liquid nitrogen to stop the evolution of the Zr oligomerization during XAS measurements. In this second series, the *X* value was fixed at 3.

**3.5. XAS Spectra Collection.** Zr−K-edge XAS experiments were carried out at the European Synchrotron Radiation Facility (ESRF, Grenoble-France) on the BM32 beamline with Si (111) monochromator crystals, using the fluorescence detection mode due to the very low concentration of Zr in liquid or gel samples (only 37 ppm for the lowest Zr concentration). The storage ring was operated at 6 GeV with a current of 200 mA. The size of the X-ray source was 0.4 × 0.2 mm. By combining the high brilliance from the ESRF synchrotron source with a multichannel fluorescence detector (30 Ge detectors) and 6 h scan for each spectrum, we were able to obtain spectra with a very high signal/noise ratio for even the lowest Zr concentrations. XAS spectra were scanned from 100 eV below to 800 eV above the Zr−K-edge.

**3.6. XAS Spectra Analysis.** *3.6.1. Normalization of XANES Spectra.* The pre-edge part was extracted from the XANES (X-ray absorption near edge structure) region (extended from 17950 to 17990 eV). XANES spectra intensity were normalized by fitting the photoelectric background above the absorption edge with a 2nd order polynomial function.

*3.6.2. EXAFS Analysis.* The data reduction was done using a series of programs developed by Michalowicz,[28] based on standard procedures.[29] The extracted EXAFS was $k^2$ weighted (with $k$ = wave vector) to enhance the high-$k$ region and Fourier transformed over the $k$ range of 2.4 to 14−15 Å$^{-1}$ to $R$ space, using a kaiser apodization window with $\tau = 2.5$. The resulting pseudoradial distribution functions (RDF) are uncorrected for phase shift, leading to a shift of the peaks by 0.3−0.4 Å. Separate peaks in the RDF corresponding to successive shells of neighboring atoms around zirconium were isolated by Back−Fourier transformation for single or multiple shell analysis. The analysis of partial $\chi(k)$ was based upon the curved wave EXAFS formalism[30] in the single scattering approximation. Curve fitting was performed with a non linear least-squares procedure, and phase ($\phi_{backscatterer}(k)$, $\delta_{central\ atom}(k)$) and amplitude ($|f_{backscatterer}(\theta, k, R)|$) functions used were calculated with FEFF7.[31] These functions for Zr−O, Zr−C, and Zr−Zr were tested on the spectra of $ZrOCl_2 \cdot 8H_2O$, Zr−acetylacetone (Zr−acac), Zr-$(C_4H_9O)_4$ (Zr−butoxide), and $ZrSiO_4$. Structural parameters ($R_i$ (distances between Zr and neighbor atoms), $N_i$ (number of neighbors)) calculated by EXAFS modeling were in good agreement with X-ray diffraction (XRD) data (Table 1). $\Delta E_0$ values derived from EXAFS calculations for the several scattering paths were 0.0, 18, and −2 eV for Zr−O, Zr−C, and Zr−Zr, respectively. The $\Delta E_0$ parameter corresponds to the difference between the threshold energy value for the mineral compounds and the value used by FEFF7. During modeling of experimental EXAFS spectra of unknown samples, these $\Delta E_0$ values will be used and kept constant. The high $\Delta E_0$ value for the Zr−C atomic shell is consistent with previous findings ($\Delta E_0$ = 20 eV[32] and 22−24 eV[17]). For each atomic shell of the unknown samples, interatomic distance $R$, coordination number $N$, and Debye−Waller factor $\sigma$ (which accounts for thermal vibrations and static disorder) were adjusted. The limit on the number of free parameters ($N_{ind} = (2\Delta k\, \Delta R)/\pi$) was in no case exceeded. Errors for the distance and coordination number are ±0.02 and ±20%, respectively.

FEFF7 calculations were also performed to estimate the contribution of multiple scattering (MS) paths on the EXAFS signal. A test was done on the partial EXAFS spectrum (2.2−4.3 Å range of the RDF) of Zr−acac. The MS calculation is detailed elsewhere.[35] The EXAFS parameters calibrated during the MS calculation of the EXAFS spectrum of Zr−acac were used to calculate the MS contributions for the EXAFS spectrum of the Zr−lactate stock solution.

**3.7. Quantum Mechanical Calculations.** Quantum mechanical calculations have been performed in which density functional theory (DFT) was applied, using the Jaguar suite of programs.[36] The hybrid B3LYP functional[37,38] in combination with the following tailor-made basis set (C, H, 6-31G(d,p); O, 6−31+G(d,p); and Zr, LanL2DZ[39]) was used for geometry optimizations. These calculations were subsequently followed by a calculation of the vibrational modes to confirm the desired state of the obtained stationary point on the potential energy surface and to include entropic contributions. The pseudospectral method has been applied in all calculations to speed up the calculations, e.g., the $Zr_2lactate_6(OH)_2$ complex is described by 816 basis functions with this mixed basis set.

## 4. Results and Discussion

**4.1. Determining the First Coordination Sphere of Zr Lactate and Zr-Gels from XANES Results.** Analysis of the XANES region is very sensitive to the geometry of the first coordination sphere of the absorbing element. Several studies[16,40] of XANES at the Zr−K edge have demonstrated the efficiency of this technique in differentiating Zr hexa- from hepta- or octa-coordinated spheres. Figure 1 presents the effects of various Zr coordination spheres on the modifications of XANES. The shape of the absorption-edge peak at 18025 eV (s → p electronic transition), also known as the white line, changes between hexacoordinated Zr samples (Zr−N, Zr−butoxide) and Zr in a dodecahedral symmetry (Zr−acac, $ZrOCl_2 \cdot 8H_2O$). Moreover,

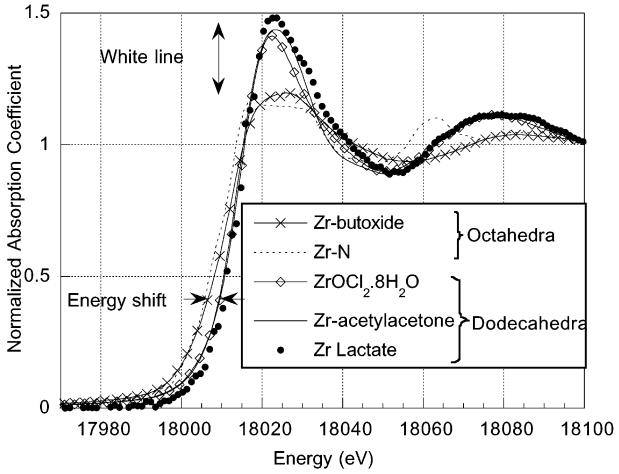


**Figure 1.** Normalized XANES spectra of Zr samples compared with spectra of model compounds.

a shift in energy exists between both symmetries (see arrows Figure 1). This shift, measured from the maximum of the first derivative of the normalized XANES, is −4.5 eV for the 6-fold coordinated Zr samples compared to the 8-fold samples.

The XANES spectra for all zirconium lactate solutions and zirconium−HSPAM gels we have analyzed are similar to the spectra of 8-fold-7-fold-coordinated Zr samples (Figure 1). Thus, seven or eight oxygen atoms are present in the first coordination sphere of Zr in our conditions.

**4.2. Zirconium Complexes in Lactate Solutions.** *4.2.1. Zirconium Atomic Environment of the Zirconium Lactate Stock Solution, Derived from EXAFS Analysis and Coupled to DFT Calculations.* Figure 2 and Table 2 present the calculated partial EXAFS spectra and derived structural parameters: R (interatomic distance), N(number of atoms around Zr) and $\sigma$ (debye-weller factor). The first coordination sphere was recalculated with two oxygen atomic shells. We found that on average 0.6 oxygen atoms are located at 2.01 Å and 7.4 are at 2.18 Å from the $Zr^{4+}$ ion. This is in agreement with XANES results, which shows that the zirconium is in a dodecahedral environment in all analyzed samples.

The RDF area between 2.18 and 3.78 Å was calculated with three atomic shells. This calculation is statistically correct, because the number of independent parameters, $N_{ind}$, is 13, and three parameters have been adjusted for each atomic shell, $N$, $R$, and $\sigma$.

The resulting fit indicates that 7.3(±1.6) carbon atoms are present around Zr at 2.76 and 3.20 Å. These Zr−C contributions could be related to Zr−O−C linkages. In the case of Zr-(chelate)$_4$, eight carbon atoms are located at distances lower than 3.30 Å (this is the case for Zr−(acac)$_4$[40]). Because the lactate/zirconium molar ratio in the stock solution equals 3, and that lactate is a chelate, it can be suggested that three lactate ligands surround each Zr(Figure 3).

The presence of Zr atoms at 3.54 Å certainly corresponds to Zr $\langle^{OH}_{OH}\rangle$ Zr linkages. For reference compounds, this type of linkage leads to Zr−Zr distances in the 3.48−3.64 Å range.[9,15,34,41,42] Thus, we can reasonably conclude that oligomeric Zr species are formed through Zr $\langle^{OH}_{OH}\rangle$ Zr linkages. The fact that the number of zirconium atoms $N_{Zr}$ at 3.58 Å, is 1.0-(±0.2) could mean that dimers are formed. It therefore seems that $Zr_2$−lactate$_6$ species are present in the stock solution.

To validate the hypothesis of the presence of $Zr_2$−lactate$_6$ dimer in the stock solution, the interatomic distances obtained from the DFT calculations for the $Zr_2$−lactate$_6$ cluster (Figure 3) are compared with the EXAFS results (Table 3). Zr−$O_{carb}$ equals oxygen from a carboxylate group, Zr−$O_{hydxyl}$ equals oxygen from a hydroxyl group, Zr−$O_{hydxid}$ equals Oxygen from a hydroxide group (bridging hydroxide), Zr−$C_{carb}$ equals carbon from a carboxyl group, and Zr−$C_{hydxyl}$ equals carbon from a hydroxyl group. We have also modeled the $Zr_2$−lactate$_6$(OH)$_6$ complex in which the lactate ligands were bound to the Zr in a monodentate fashion and in which water molecules occupy the "created" vacancies: $Zr_2$−lactate$_6$($H_2O$)$_6$(OH)$_2$. However, the geometrical parameters of this complex do not correspond at all to the EXAFS data. For example, the Zr−$C_2$ distance in this complex is 4.5 Å. That clearly shows that lactate ligands are not linked through monodentate fashion.

The interatomic distances obtained from the B3LYP optimized geometry, shown in Figure 3 and for which the lactates are bound in a bidentate fashion, are compared with EXAFS data in Table 3. The analysis of the Zr−O and Zr−C B3LYP distances suggests that the structural disorder is relatively high. The Zr−O distances vary between 2.08 and 2.53 Å, and the Zr−C distances vary between 3.07 and 3.39 Å. However, the different DFT contributions are not easily comparable with EXAFS data. XAFS spectra never reflect anything but a population-weighted average for the target element. Thus, the comparison must be done between averaged Zr−O and Zr−C interatomic distances from DFT and EXAFS results.

The average of the different atomic shells should follow some rules. Because EXAFS calculation can differentiate 2 Zr−O or Zr−C shells only if $\Delta R > \pi/2k_{max} = 0.11$ Å (with $k_{max} = 14.0$ Å$^{-1}$ (beat-node method[29])), two Zr−O contributions seem to exist from B3LYP calculations (Table 3). The first contribution corresponds to 4.5 oxygen atoms at 2.13 Å, and the second corresponds to 3.5 oxygen atoms at 2.39 Å. The result is relatively different from interatomic distances determined from EXAFS calculations, because 7.4 oxygen atoms are located at 2.18 Å from Zr ($\sigma = 0.086$ Å) and 0.6 oxygen atoms are at 2.01 Å ($\sigma = 0.055$ Å). Thus, from B3LYP calculations, it seems that two distances exist, whereas in the case of EXAFS, almost all oxygen atoms are at 2.18 Å. If the two B3LYP Zr−O contributions are averaged, the result indicates that 8 oxygen atoms are located at $\bar{R} = 2.24$ Å with a standard deviation

$$\sigma = 0.14 \text{ Å} = \left(\frac{1}{n}\sum_{n}^{i=1} R_i^2 - (\bar{R})^2\right)^{1/2} \quad (n = 16)$$

Thus, B3LYP overestimates not only the Zr−O distances but also the structural disorder. However, it is not certain that the structure of the dimer as modeled here is the actual species found in aqueous solution. Most probably, the whole complex is negatively charged, i.e., some of the hydroxyl groups of the lactate have their proton dissociated. This is, in fact, what is modeled for the monomer species with the B3LYP functional. Also, zirconium tetra-lactate is likely to have a negative net charge. Because the Zr−O(hydroxyl) distance is significantly smaller if the protons of the hydroxyl group are dissociated (typical values are 2.3 Å with proton and 2.1 Å without proton), the average Zr−O distance becomes smaller and consequently could come very close to the experimental value. A more detailed theoretical study that includes the structural aspects, which we just briefly mentioned here are taken into account for the monomer and dimer of zirconium lactate together with some other electronic features, is to be published soon.[43]

In the case of the Zr−C distances, the discrepancy between EXAFS and B3LYP is lower. Two Zr−C contributions seem to exist from the B3LYP calculation: one at 3.115 Å (carbon

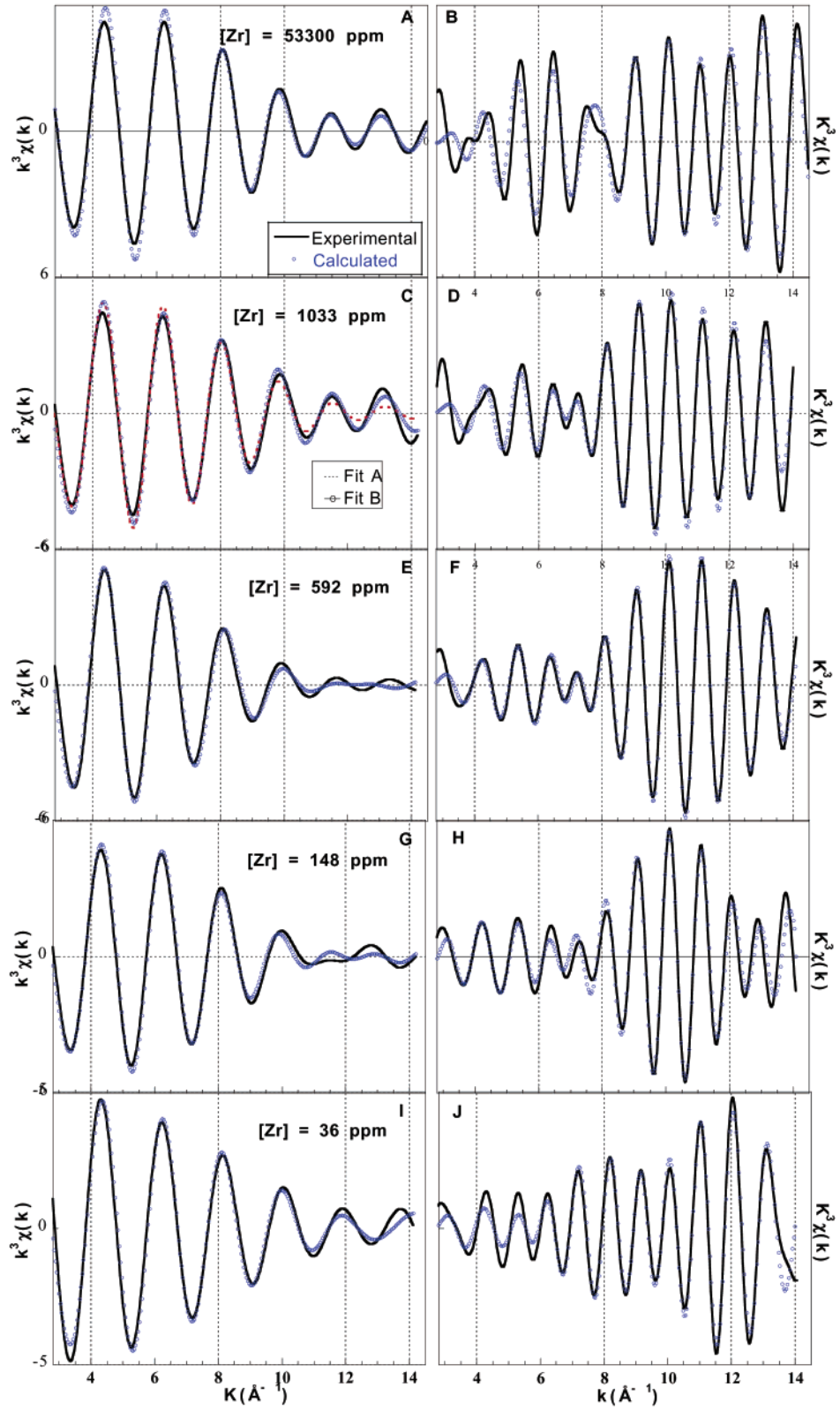


**Figure 2.** Experimental and calculated partial EXAFS spectra corresponding to the back−Fourier transforms of the different filter windows: (A) for the Zr lactate solution at 53300 ppm in Zr (filter 1), (B) for the Zr lactate solution at 53300 ppm in Zr (filter 2), (C) for the Zr lactate solution at 1035 ppm in Zr (filter 1), (D)for the Zr lactate solution at 1035 ppm in Zr (filter 2), (E) for the Zr lactate solution at 592 ppm in Zr (filter 1), (F) for the Zr lactate solution at 592 ppm in Zr (filter 2), (G) for the Zr lactate solution at 148 ppm in Zr (filter 1), (H) for the Zr lactate solution at 148 ppm in Zr (filter 2), (I) for the Zr lacate solution at 37 ppm in Zr (filter 1), (J) for the Zr lacate solution at 37 ppm in Zr (filter 2).

from carboxyl group) and another at 3.31 Å (carbon from hydroxyl group), each one corresponding to three carbon atoms. From EXAFS, two contributions exist, but almost all carbon atoms are located at 3.20 Å (Table 2). By taking into account the two Zr−C contributions obtained from B3LYP calculation in the mean average, we found that the Zr−C average distance is 3.214 Å with $\sigma = 0.104$ Å. This distance is very close to the experimental value (3.20 Å). The main difference is that B3LYP calculation is unable to reproduce the very short Zr−C contribution detected at 2.76 Å and overestimates the structural disorder.

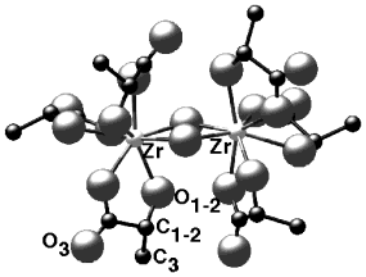


**Figure 3.** Structure of the $Zr_2$−lactate$_6$ cluster obtained from DFT calculations.

**TABLE 2: Structural Parameters Derived from EXAFS Analysis of the Zirconium Lactate Solutions Diluted at pH = 6**

| sample | filter window (Å) | fit | atomic pair | $R$ (Å) | $\sigma$ (Å) | $N$ | $Q^\theta$ |
|---|---|---|---|---|---|---|---|
| 53300 ppm | 1.23−2.04 | | Zr−$O_1$ | 2.01 | 0.055 | 0.6 | 0.017 |
| | | | Zr−$O_2$ | 2.18 | 0.086 | 7.4 | |
| | 2.22−3.80 | | Zr−$C_1$ | 2.76 | 0.012 | 1.0 | 0.180 |
| | | | Zr−$C_2$ | 3.20 | 0.065 | 6.3 | |
| | | | Zr−Zr | 3.54 | 0.062 | 1.0 | |
| 1035 ppm | 1.21−2.02 | N°1 | Zr−O | 2.17 | 0.098 | 7.0 | 0.029 |
| | | N°2 | Zr−$O_1$ | 1.99 | 0.108 | 2.0 | 0.020 |
| | | | Zr−$O_2$ | 2.17 | 0.080 | 6.0[a] | |
| | 2.23−3.84 | | Zr−$C_1$ | 2.72 | 0.014 | 0.3 | 0.117 |
| | | | Zr−$C_2$ | 3.15 | 0.085 | 5.1 | |
| | | | Zr−Zr | 3.53 | 0.075 | 1.9 | |
| 592 ppm | 1.16−2.08 | | Zr−$O_1$ | 2.03 | 0.008 | 0.3 | 0.020 |
| | | | Zr−$O_2$ | 2.16 | 0.097 | 6.8 | |
| | 2.37−3.65 | fit A | Zr−$C_1$ | 2.83 | 0.008 | 0.6 | 0.075 |
| | | | Zr−$C_2$ | 3.11 | 0.087 | 4.5 | |
| | | | Zr−Zr | 3.57 | 0.077 | 1.8 | |
| 148 ppm | 1.19−2.07 | | Zr−$O_1$ | 2.04 | 0.057 | 0.7 | 0.032 |
| | | | Zr−$O_2$ | 2.17 | 0.102 | 7.0 | |
| | 2.40−3.62 | | Zr−$C_1$ | 2.78 | 0.020 | 0.2 | 0.033 |
| | | | Zr−$C_2$ | 3.16 | 0.050 | 3.5 | |
| | | | Zr−Zr | 3.53 | 0.085 | 2.4 | |
| 37 ppm | 1.02−2.01 | | Zr−$O_1$ | 1.83 | 0.017 | 0.3 | 0.019 |
| | | | Zr−$O_2$ | 2.14 | 0.109 | 7.7 | |
| | 2.18−3.75 | | Zr−$C_1$ | 2.95 | 0.010 | 1.4 | 0.048 |
| | | | Zr−$C_2$ | 3.24 | 0.075 | 2.9 | |
| | | | Zr−Zr | 3.55 | 0.090 | 2.9 | |

[a] $NO_1 + NO_2 = 8$.

The effect of MS on the EXAFS spectrum of the zirconium lactate stock solution was estimated and confirmed the results obtained from the single scattering EXAFS analysis. Details of the EXAFS MS calculations are detailed elsewhere.[35]

*4.2.2. Zirconium Speciation in Diluted Zirconium Lactate Solutions.* Because dilutions have been completed at constant pH, the significant change is a decrease in lactate concentration, while the OH concentration remains constant. In other terms, the lactate to hydroxyl ratio decreases.

Figure 4 a shows the different EXAFS spectra of zirconium lactate solutions at pH = 6 after a constant aging time of 20 min after dilution for the following Zr concentrations: 53300, 1035, 592, 148, and 37 ppm. There are no major differences, suggesting that the atomic environment of Zr does not drastically change 20 min after dilution. However, frequency shifts at 3.7−3.9 and 6.5−6.7 Å$^{-1}$ exist between the stock solution ([Zr] = 53300 ppm) and the other solutions, suggesting modifications in the atomic environment of Zr.

These slight differences in frequency can be visualized on the RDF (Figure 4 b). The intensities and the maxima of the peaks in the 2.3−2.9 Å RDF area (distances are uncorrected for the phase shift) in the stock solution spectrum are different from those found in the more diluted solution spectra. Moreover, the position of the peak at 3.4 Å shifts to ≈3.15 Å when the solutions are diluted. The interpretation of these changes in term of structure requires modeling of the EXAFS spectra.

Table 2 shows the EXAFS structural parameters calculated for the 4 diluted solutions (Figure 2). The analysis of the first coordination sphere confirms the XANES results: Zr remains in a dodecahedral environment in dilute solutions. The dilution does not seem to change zirconium coordination after 20 min of aging.

However, the analysis of the second coordination sphere revealed an oligomerization of the zirconium. Indeed, dilution of the zirconium lactate solution leads to an increase in the number of neighbor zirconium ions ($N_{Zr}$) at distances between 3.5 and 3.6 Å. This atomic contribution corresponds to Zr $\langle{}^{OH}_{OH}\rangle$ Zr linkages. A decrease in the concentration of the stock solution down to the more diluted solutions leads to an increase in $N_{Zr}$ from 1.0 to 1.9, 1.8 (fit A), 2.4, and 2.9 for the 53300, 1035, 592, 148, and 37 ppm solutions, respectively. This increase indicates a progressive oligomerization of the zirconium species, caused by dilution. The exact structure is difficult to determine from EXAFS results alone. Several 3D structures could be associated with one set of EXAFS data. Let us examine the case of the Zr 1035 ppm solution for which $N_{Zr} = 1.9$. The

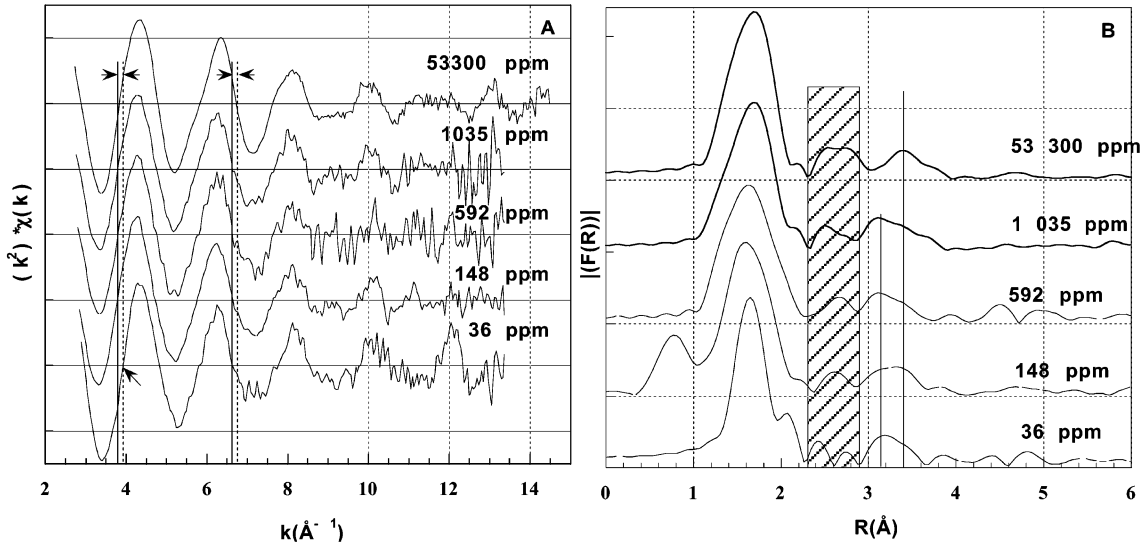


**Figure 4.** (a) EXAFS spectra and (b) RDF's of the Zr lacate diluted solutions at pH = 6.

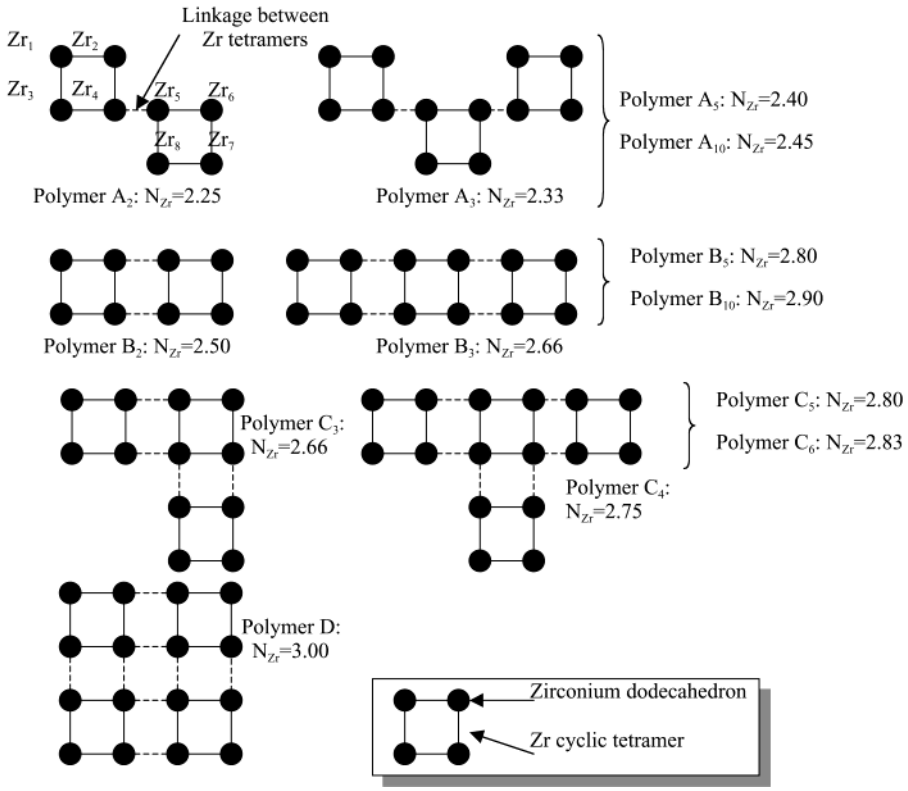


**Figure 5.** Examples of cyclic tetramer linkages: polymer from the A type, 1 Zr $\langle^{OH}_{OH}\rangle$ Zr linkage (doted line); polymer from the B type, 2 Zr $\langle^{OH}_{OH}\rangle$ Zr linkages and linear structure; and polymer from the C and D types, multi Zr $\langle^{OH}_{OH}\rangle$ Zr linkages.

**TABLE 3: Comparison between Interatomic Distances for $Zr_2Lactate_6$ Cluster-Obtained by DFT Calculations and EXAFS Modeling of the Concentrated Stock Zr Lactate Solution**

| atomic pair | DFT interatomic dist (Å) (site 1) | DFT interatomic dist (Å) (site 2) | DFT avg (Å) | DFT avg (Å) | EXAFS (Å) |
|---|---|---|---|---|---|
| | | 1st coordination sphere | | | |
| Zr−$O_{carb}$ | 2.10 | 2.076 | 2.127*4.5 | 2.242*8 | 2.01*0.6 = Zr−$O_1$ |
| Zr−$O_{carb}$ | 2.12 | 2.10 | | | |
| Zr−$O_{carb}$ | 2.14 | 2.12 | | | |
| Zr−$O_{hydixd}$ | 2.15 | 2.22 | | | |
| Zr−$O_{hydxid}$ | 2.12 | 2.30 | 2.388*3.5 | | 2.18*7.4 = Zr−$O_2$ |
| Zr−$O_{hydxyl}$ | 2.38 | 2.33 | | | |
| Zr−$O_{hydxyl}$ | 2.40 | 2.36 | | | |
| Zr−$O_{hydxyl}$ | 2.53 | 2.42 | | | |
| | | 2nd coordination sphere | | | |
| Zr−$C_{carb}$ | 3.11 | 3.07 | 3.115*3 | 3.214*6 | 2.76*1.0 = Zr−$C_1$ |
| Zr−$C_{carb}$ | 3.13 | 3.12 | | | |
| Zr−$C_{carb}$ | 3.13 | 3.13 | | | |
| Zr−$C_{hydxyl}$ | 3.27 | 3.27 | 3.310*3 | | 3.20*6.3 = Zr−$C_2$ |
| Zr−$C_{hydxyl}$ | 3.33 | 3.29 | | | |
| Zr−$C_{hydxyl}$ | 3.39 | 3.33 | | | |
| Zr−Zr | 3.59 | 3.59 | 3.59 | | 3.54 |

structure of the cyclic tetramer (Figure 5) that was previously detected during the hydrolysis of Zr salts[8,13,44] could correspond to this EXAFS result, because, in this molecule, each Zr is surrounded by two other Zr's at a distance of 3.5−3.6 Å. However, a linear zirconium polymer constituted by a high number of Zr dodecahedra would also give a similar EXAFS result. For example, a polymer constituted by 10 Zr dodecahedra would correspond to $N_{Zr} = 1.8$. EXAFS is thus unable to determine the cluster size, but in line with the literature, we will assume the formation of cyclic tetramers is more likely than that of linear structures.

When it is considered that the cyclic Zr tetramer may be formed at 1035 ppm, $N_{Zr}$ values higher than 2 for the more dilute solutions could indicate that these cyclic tetramers are linked with each other to form aggregates. For example, if two cyclic tetramers share one edge (Figure 5), the theoretical EXAFS analysis of this sample would lead to $N_{Zr} = 2.25$. The calculation of $N_{Zr}$ is obtained as follows: Six Zr's are linked to two others ($Zr_{1\rightarrow3,6\rightarrow8}$) and two Zr's are linked to three others ($Zr_4$ and $Zr_5$). Then the average EXAFS $N_{Zr} = 2.25 = (6_{Zr} \times 2 + 2_{Zr} \times 3)/8_{Zr}$. Hence, by assumption of different type of linkages between Zr cyclic tetramers, it seems possible to infer

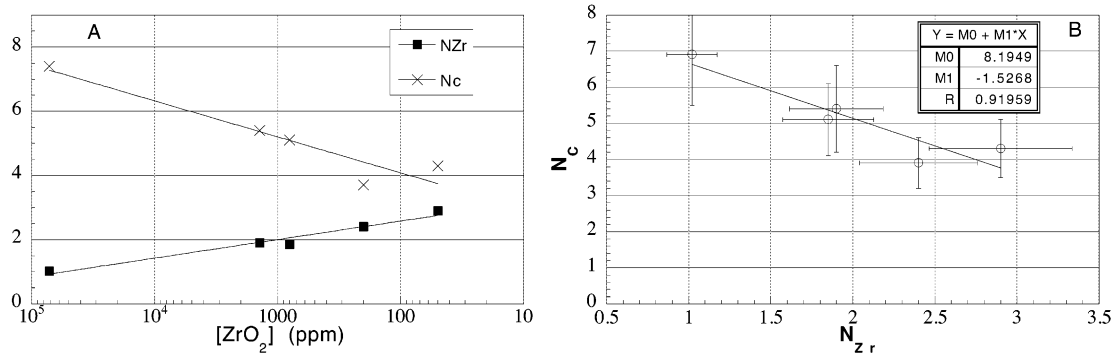


**Figure 6.** Evolution of $N_{Zr}$ (number of Zr atoms around Zr atom), $N_{C1+2}$ (number of carbon atoms around Zr atoms) versus Zr concentration, and correlation between $N_{Zr}$ and $N_{C1+2}$ for the Zr lactate solutions.

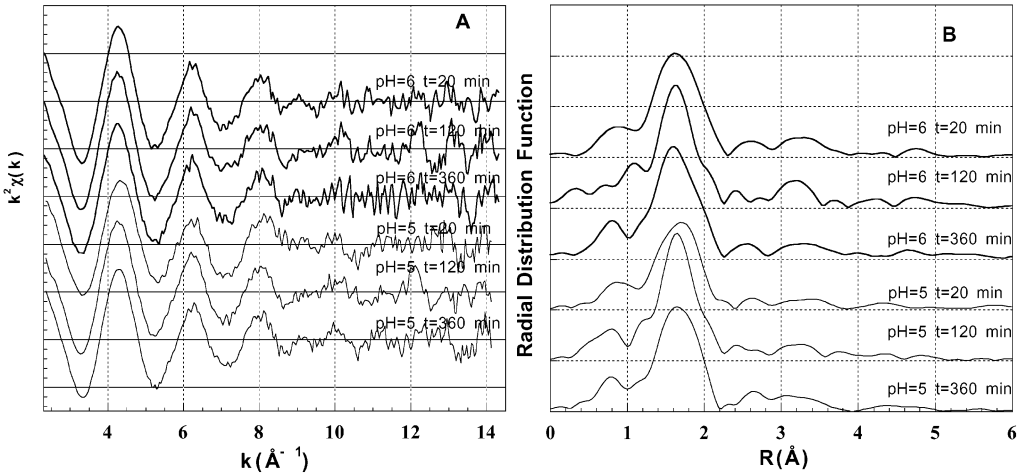


**Figure 7.** EXAFS and RDF for the Zr lacate solutions at 74 ppm at various aging time and at pH = 5 and 6.

from EXAFS an estimated size for Zr polymers. Figure 5 gives $N_{Zr}$ for different types of linkages between Zr tetramers. Even if it is difficult to determine the structure, all experimental $N_{Zr}$ values are lower than 2.9 for Zr−La solutions between 592 and 37 ppm Zr. Except in the case of polymers of type A (Figure 5), an $N_{Zr}$ value of 2.9 corresponds to small aggregates, smaller than 10 cyclic tetramers linked to each other. Hence, it seems that the oligomers present in the solution are, on average, of small size. Moreover, the polymers of type A appear less probable than the other types. It seems difficult to imagine an infinite linear polymer in solution. When these linear polymers reach a certain size, the probability of contact with another linear polymer increases. Thus, contact between linear polymers leads to an increase in the connectivity of the polymer, and $N_{Zr}$ increases consequently. This new polymer formed from the linkage between two polymers of type A could certainly be of type B or C. In our case, this growth mechanism through multiple linkages between cyclic tetramers (polymers of type B, C, and D) is hypothetical and based on the initial formation of the cyclic tetramer. Turillas et al.[27] and Sanchez and In[40] proposed the same growth mechanism to explain the gel formation of zirconium hydroxide, which reinforces our interpretation.

Concerning the carbon atoms around zirconium, the decrease in the total number of carbons ($N_C$) with dilution from 6 to 7 down to 4 is correlated with an increase of $N_{Zr}$ from 1 up to 2.9. Figure 6a illustrates the relationship between $N_{Zr}$ and $N_C$ during the dilution and the relationship between $N_{Zr}$ and $N_C$ for all zirconium lactate solutions (Figure 6 b). Even though the errors on $N$ and, especially, $N_C$ are relatively high due to the low intensity of the Zr−C EXAFS amplitude function as compared with that of Zr−Zr, there is clearly a correlation

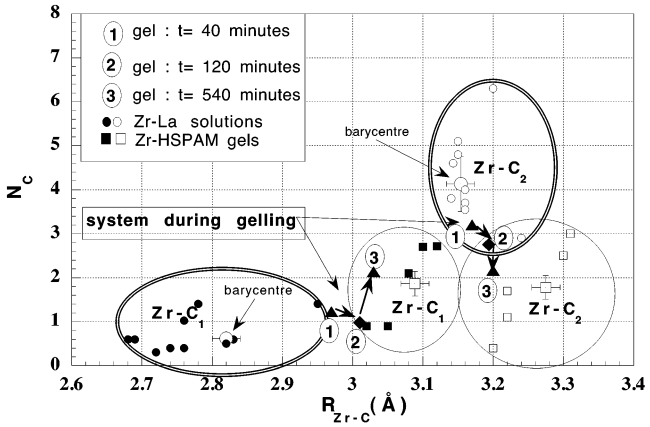


**Figure 8.** $R_{Zr-C}$ (Zr−C interatomic distance) versus $N_C$ (number of carbon atoms around Zr atoms) for all the Zr lactate solutions and Zr−gels.

between the increase in $N_{Zr}$ and the decrease in $N_C$. That suggests that one bidentate lactate ligand is progressively replaced by one Zr $\langle^{OH}_{OH}\rangle$ Zr linkage as dilution increases.

*4.2.3. Effect of pH on Zirconium Oligomerization Kinetics.* Figure 7 presents the EXAFS and RDF results corresponding to the zirconium lactate solutions at pH 6 and 5 as a function of time. It appears that the EXAFS spectra are quite similar from $k = 2.5$ to 8.4 Å$^{-1}$. In addition, the qualitative analysis of RDF gave the same result, i.e., the polymerization of zirconium species does not change very quickly with time.

The results of the EXAFS analysis are detailed in Table 4. The first coordination sphere does not change with time for a diluted zirconium lactate solution at pH = 6. This result is in

**TABLE 4: Structural Parameters Derived from EXAFS Analysis of the Zirconium Lactate Solutions (74 ppm in Zr) Diluted at pH = 6 and pH = 5**

| samples | filter window (Å) | atomic pair | $R$ (Å) | $\sigma$ (Å) | N | Q |
|---|---|---|---|---|---|---|
| zirconium lactate solutions at pH = 6 and 74 ppm | | | | | | |
| t = 20 min | 1.20−2.15 | Zr−$O_1$ | 2.15 | 0.092 | 6.8 | 0.042 |
| | | Zr−$O_2$ | 2.30 | 0.015 | 1.2 | |
| | 2.35−3.80 | Zr−$C_1$ | 2.75 | 0.016 | 0.4 | 0.090 |
| | | Zr−$C_2$ | 3.16 | 0.068 | 4.0 | |
| | | Zr−Zr | 3.57 | 0.060 | 1.0 | |
| t = 120 min | 1.20−2.15 Å | Zr−$O_1$ | 2.16 | 0.084 | 6.6 | 0.061 |
| | | Zr−$O_2$ | 2.33 | 0.048 | 1.4 | |
| | 2.24−3.85 | Zr−$C_1$ | 2.78 | 0.010 | 0.9 | 0.075 |
| | | Zr−$C_2$ | 3.15 | 0.075 | 3.1 | |
| | | Zr−Zr | 3.54 | 0.034 | 1.0 | |
| t = 360 min | 1.20−2.15 Å | Zr−$O_1$ | 2.15 | 0.090 | 6.4 | 0.052 |
| | | Zr−$O_2$ | 2.30 | 0.047 | 1.6 | |
| | 2.24−3.88 | Zr−$C_1$ | 2.73 | 0.020 | 0.5 | 0.150 |
| | | Zr−$C_2$ | 3.14 | 0.096 | 4.8 | |
| | | Zr−Zr | 3.57 | 0.100 | 2.4 | |
| zirconium lactate solutions at pH = 5 and 74 ppm | | | | | | |
| t = 20 min | 2.35−3.74 | Zr−$C_1$ | 2.82 | 0.010 | 0.6 | 0.092 |
| | | Zr−$C_2$ | 3.13 | 0.086 | 3.4 | |
| | | Zr−Zr | 3.58 | 0.064 | 1.2 | |
| t = 120 min | 2.35−3.74 | Zr−$C_1$ | 2.69 | 0.016 | 0.4 | 0.200 |
| | | Zr−$C_2$ | 3.15 | 0.104 | 4.9 | |
| | | Zr−Zr | 3.54 | 0.055 | 0.9 | |
| t = 360 min | 2.37−3.72 | Zr−$C_1$ | 2.82 | 0.040 | 0.5 | 0.085 |
| | | Zr−$C_2$ | 3.12 | 0.042 | 3.5 | |
| | | Zr−Zr | 3.56 | 0.102 | 2.2 | |

agreement with previous analyses of diluted samples at various concentrations (cf. Table 3).

The analysis of the second coordination sphere indicates a slight modification of the atomic environment of Zr. For the solutions at pH = 6, the increase of $N_{Zr}$ from 1.0 to 2.4 after 360 min of aging suggests that oligomerization does take place but that, in solution, only small clusters exist. In light of the previous discussion concerning $N_{Zr}$ determined by EXAFS and the size of the Zr oligomers, clusters in solution should be limited to two or three cyclic tetramers. This evolution of Zr species does not seem to be correlated to the number of carbon atoms, which remains constant. All these observations suggest a low level of oligomerization, even after 360 min. At pH = 5, it seems that the oligomerization of Zr is still slower, remaining at a lower level than at pH = 6. At $t$ = 20 and 120 min, the solution is identical to that of the stock solution. After 360 min of aging at 20 °C and pH = 5, a fraction of zirconium was oligomerized. From $N_{Zr}$ = 2.2, we concluded that tetramers and oligomers constituted by two tetramers could be formed.

**4.3. Zirconium Complexes in HSPAM Gels.** *4.3.1. Influence of pH on the Speciation of Zirconium Within Polymer Gels and Kinetics Aspects.* The influence of pH has been tested in a first series of experiments (first series: gels formed at pH = 6 and 7 after 5 days, with $X$ = 6). The gel obtained at pH = 6 with $X$ = 6 and analyzed after 5 days of aging certainly contains Zr dimers as cross-linkers, because $N_{Zr}$ = 1.2. In this case, it seems that oligomerization was hindered by HSPAM. For the same gel formed at pH = 7, $N_{Zr}$ = 2.3 after 5 days. In this case, the cross-linking species could be cyclic tetramers or, alternatively, only a small number of dimers have been used to cross-link polymers, while the majority is oligomerized. Thus, the oligomerization of Zr is faster at higher pH. Gelling kinetics have also been found to be strongly diminished with increasing pH.[3−5] Such a delay in gelling is consistent with Zr oligomerization, but the major effect is likely a decrease in the reactivity of dimers or tetramers when OH groups replace lactate.

In the second series of experiments, the gels were formed at pH = 6 with $X$ = 3 and observed at various aging times (40, 240, and 540 min). The evolution of $N_{Zr}$ suggests that the oligomerization of Zr is much slower than that in Zr lactate solutions but faster than that in the first series of experiments with $X$ = 6. Forty minutes after the mixing between zirconium lactate and HSPAM solutions, it seems that Zr species are a mixture of dimers and tetramers, because $N_{Zr}$ = 1.5, whereas dimers are present in zirconium lactate just before the mixing (cf., section 4.2.3., Table 4). This oligomerization could be due to a dilution of the initial zirconium lactate solution at 74 ppm before the mixing with the HSPAM solution. Because the mixing is done with a 50/50 volume ratio, the Zr concentration decreases from 74 to 37 ppm in Zr. In a second step, the oligomerization seems to be blocked, or at least hindered, by the gelling process, because after 120 min, $N_{Zr}$ has not increased. After 540 min (9 hours) the oligomerization of Zr leads to the formation of a larger number of tetramers, as suggested by the value $N_{Zr}$ = 1.8.

*4.3.2. Exchanges Between Lactate and Acrylate Ligands While Gelling.* The Zr−C interatomic distances determined for the HSPAM gels after 5 days at pH = 6 and 7 days with $X$ = 6 (Table 5) are different from those determined in the Zr lactate solutions analyzed (cf., Tables 2 and 5). Although the majority of carbon atoms are located at 3.15−3.20 Å from the Zr in the Zr−La solutions (Tables 2 and 4), this range is expanded from 3.06 to 3.30 Å in the case of Zr−HSPAM gels (Table 5). This change can be attributed to ligand exchange between lactate and acrylate groups fixed on HSPAM.

To better understand the modification of the atomic environment of Zr during gelation, a statistical study of the structural parameters determined by EXAFS was performed. Figure 8 presents the different Zr−C contributions detected by EXAFS for all the Zr lactate solutions and gels with $N_C$ on the $y$ axis versus $R_{Zr-C}$ on the $x$ axis. We also added some data from Zr−HSPAM gels detailed elsewhere.[35] This statistical analysis included the two Zr−C contributions: one at short Zr−C distance (Zr−$C_1$) and another at longer Zr−C distance (Zr−$C_2$).

These two contributions, reported in Figure 8, are clearly distinct for the Zr lactate solutions. The average distance in zirconium lactate solutions for Zr−$C_1$ populations is 2.82 Å with a mean value $N_{C1}$ = 0.62, and the average distance for Zr−$C_2$ is 3.154 Å with $N_{C2}$ = 4.13 (average). In the case of the Zr−HSPAM gels, these two populations are shifted at 3.089 Å with $N_{C1}$ = 1.86 and 3.275 Å with $N_{C2}$ = 1.78. Even if the 2nd coordination sphere of Zr contains C atoms, it is surprising that it is possible to distinguish Zr lactate solutions from Zr−HSPAM gels. This result shows that, in our case, EXAFS results are sensitive enough to detect ligand exchange between lactate and acrylate. Moreover, it is interesting to observe that the position of the two Zr−C populations for the gels that are not completely formed (second series of experiment gels at $X$ = 3 and after 40, 120, and 540 min of aging (or gelling) time, Table 5), are between the group of Zr lactate and Zr−HSPAM gels points. When the gelling time increases, the Zr−$C_1$ and Zr−$C_2$ points evolve from the Zr lactate to the Zr−HSPAM gels point group (arrows Figure 8). This result shows that the EXAFS analysis is sensitive enough to follow the gelling kinetics, i.e., the exchange between lactate and acrylate around Zr. Moreover, it seems that this exchange is not complete for gels in formation

**TABLE 5: Structural Parameters Derived from EXAFS Analysis of the HSPAM Gels**

| sample | filter window (Å) | atomic pair | $R$ (Å) | $\sigma$ (Å) | $N$ | $Q$ |
|---|---|---|---|---|---|---|
| HSPAM gels at pH = 6 and pH = 7 with $X = 6^a$ after 5 days of aging time | | | | | | |
| pH = 6 | 1.28−2.04 | Zr−$O_1$ | 2.17 | 0.094 | 6.8 | 0.009 |
| | | Zr−$O_2$ | 2.36 | 0.076 | 1.2 | |
| | 2.44−3.52 | Zr−$C_1$ | 3.12 | 0.040 | 2.7 | 0.036 |
| | | Zr−$C_2$ | 3.30 | 0.040 | 2.5 | |
| | | Zr−Zr | 3.55 | 0.068 | 1.2 | |
| pH = 7 | 1.23−2.04 Å | Zr−$O_1$ | 2.16 | 0.089 | 5.7 | 0.004 |
| | | Zr−$O_2$ | 2.30 | 0.112 | 2.3 | |
| | 2.26−3.64 Å | Zr−$C_1$ | 3.00 | 0.110 | 2.4 | 0.073 |
| | | Zr−$C_2$ | 3.21 | 0.014 | 0.3 | |
| | | Zr−Zr | 3.55 | 0.091 | 2.3 | |
| HSPAM gels at pH = 6 at various aging time X = 3 | | | | | | |
| t = 40 min | 1.20−2.04 | Zr−$O_1$ | 2.16 | 0.097 | 6.6 | 0.009 |
| | | Zr−$O_2$ | 2.35 | 0.091 | 2.3 | |
| | 2.27−3.76 Å | Zr−$C_1$ | 2.97 | 0.012 | 1.2 | 0.066 |
| | | Zr−$C_2$ | 3.17 | 0.020 | 3.2 | |
| | | Zr−Zr | 3.53 | 0.057 | 1.5 | |
| t = 120 min | 1.16−2.09 | Zr−$O_1$ | 2.13 | 0.078 | 4.2 | 0.006 |
| | | Zr−$O_2$ | 2.28 | 0.104 | 3.7 | |
| | 2.27−3.56 Å | Zr−$C_1$ | 3.01 | 0.054 | 1.0 | 0.043 |
| | | Zr−$C_2$ | 3.19 | 0.010 | 2.8 | |
| | | Zr−Zr | 3.53 | 0.062 | 1.4 | |
| t = 540 min | 1.23−2.06 | Zr−$O_1$ | 2.16 | 0.100 | 6.6 | 0.014 |
| | | Zr−$O_2$ | 2.37 | 0.085 | 1.3 | |
| | 2.24−3.76 Å | Zr−$C_1$ | 3.03 | 0.020 | 2.1 | 0.074 |
| | | Zr−$C_2$ | 3.20 | 0.032 | 2.2 | |
| | | Zr−Zr | 3.54 | 0.075 | 1.8 | |

[a] $X$ = [ lactate/$ZrO_2$].

after 40 and 120 min. We can interpret this result by considering that only a small amount of Zr polymers react with HSPAM in agreement with rheological data published elsewhere[5] showing that the gels formed are very weak.

The EXAFS results concerning the lactate/acrylate exchange have been confirmed by the DFT calculations. The exchange reaction $Zr(lactate)_6(OH)_2 + 6\ H_2O + 6\ Ac^- \rightarrow ZrAc_6(OH)_2(H_2O)_6 + 6\ La^-$ is highly exothermic ($\Delta G = -97.1$ kcal/mol at 298 K) and thus favors the exchange of lactate ligands for acrylate ones. This reaction will be further detailed in De Bruin et al.[43]

## 5. Conclusions

The structure of zirconium complexes has been investigated using XAS experiments and molecular simulations in both zirconium lactate aqueous solutions and in polymer microgels where dilute zirconium lactate solutions were used as a cross-linker. The results are the following: in highly concentrated lactate solutions, the zirconium species were identified to be dimers stabilized by six bidentate lactates and remain stable over years. When lactate solutions are diluted, dimers become unstable and form tetramers, which, by association, could lead to precipitation. The kinetics of zirconium oligomerization in Zr lactate solutions was investigated as a function of pH and dilution. At pH = 6, the Zr oligomers evolve from $Zr_2$−lactate$_6$ to cyclic tetramer and then larger aggregates formed by linkages between cyclic tetramers. The increase in the number of Zr atoms around the central atom is correlated with a decrease in the number of carbons. This indicates that lactate groups are replaced by OH ligands involved in Zr $\langle^{OH}_{OH}\rangle$ Zr linkages. The kinetics of Zr oligomerization at 20 °C decreases as pH decreases. At pH = 6, oligomerization becomes detectable between 120 and 360 min, while at pH = 5, the size of the oligomers was found to be smaller at the same time. In Zr−HSPAM gels, oligomerization of Zr within the gel does not follow the same process as in pure Zr lactate solutions because of interaction between acrylate groups of the HSPAM polymers and Zr species. The Zr lactate clusters exchange lactate groups with acrylates of the HSPAM. Exchange kinetics are very slow, and after 540 min, the reaction is not complete. It seems that the Zr−dimer prevails at pH = 6, while cyclic tetramers are predominant at pH = 7. DFT calculations validate the structures of the Zr oligomers present in lactate solution as well as the exchange between lactate and acrylate ligands.

This study demonstrates that the use of a third generation radiation synchrotron enables the characterization of chemical processes not only in solution but also at very low concentration and that the kinetics of the reaction can be taken into account.

**Acknowledgment.** The authors thank IFP for supporting the studies and for permitting the publication of results. This work benefited from helpful discussions with Pr. J-P Jolivet from the university of Paris-VI (Paris-France) and Dr. A Masion from the CEREGE (Aix, France).

## References and Notes

(1) Cui, G. L.; Xia, J.; Xu, Z. H. J. Univ. Pet., China., Ed. Nat. Sci. 1992, 16(3), 40.
(2) Omari, A.; Polymer 1995, 36, 4263.
(3) Chauveteau, G.; Tabary, R.; Renard, M.; Omari, A. SPE Symposium *on Oilfield Chemistry*, **1999**, SPE 50752.
(4) Chauveteau, G.; Omari, A.; Tabary, R.; Renard, M.; Rose, J. *SPE-DOE Improved Oil Recovery Symposium*, **2000**, SPE 59317.
(5) Chauveteau, G.; Omari, A.; Tabary, R.; Renard, M.; Veerapen, J.; Rose, J. *SPE Symposium on Oilfield Chemistry*, **2001**, SPE 64988.
(6) Tobita, H.; Kumagai, M.; Aoyagi, N. *Polymer* **2000**, 481−487.
(7) Jolivet, J.-P.; In *From Solution to Oxide*; John Wiley and Sons: Paris, 2000.
(8) Clearfield, A. *Rev. Pure Applied Chem.*, **1964**, *14*, 91.

(9) Clearfield, A.; Vaughan, P. A. *Acta Crystallogr.* **1956**, *9*, 555.
(10) Johnson, J. S.; Krauss, K. A. *J. Am. Chem. Soc.* **1956**, *78*, 3937.
(11) Aberg, M. *Acta Chem. Scand.* **1977**, 171.
(12) Muha, G. M.; Vaughan, P. A. *Acta Crystallogr.* **1960**, *9*, 555.
(13) Singhal, A.; Toth, L. M.; Beaucage, G.; Lin, J. S.; Peterson, J. *J. Coll. Int. Sci.* **1997**, *194*, 470.
(14) Livage, J.; Doi, K.; Mazières, C. *J. Am.Ceram. Soc.* **1968**, *51*, 349.
(15) Clearfield, A. *J. Mater. Res.* **1990**, *5*, 161.
(16) Peter, D.; Ertel, T. S.; Bertagnolli, H. *J. Sol−gel Sci. Technol.*, **1994**, *3*, 91.
(17) Helmerich, A.; Raether, F.; Peter, D.; Bertagnolli, H.; *J. Mater. Sci.*, **1994**, *29*, 1388.
(18) InTorre, B. J.; Martell, A. E.; *J. Am. Chem. Soc.*, **1960**, *82*, 358.
(19) Peter, D.; Ertel, T. S.; Bertagnolli, H. *J. Sol−Gel Sci. Technol.* **1995**, *5*, 5.
(20) Bottero, J.-Y.; Manceau, A.; Villieras, F.; Tchoubar, D. *Langmuir* **1994**, *10*, 316.
(21) Rose, J.; Manceau, A.; Bottero, J. Y.; Masion, A.; Garcia, F. *Langmuir* **1996**, *12*, 6701.
(22) Rose, J.; Manceau, A.; Masion, A.; Bottero, J. Y. *Langmuir* **1997**, *13*, 3240.
(23) Jones, D.; Roziere, J.; Maireles-Torres, P.; Jimenez-Lopez, A.; Olivera-Pastor, P.; Rodriguez-Castellon, E.; Tomlinson, A. A. G. *Inorg. Chem.* **1995**, *34*, 4611.
(24) Roussel, H.; Briois, V.; Elkaim, E.; de Roy, A.; Besse, J. P. *J. Phys. Chem. B* **2000**, *104*, 25, 5915.
(25) Michot, L. J.; Montarges-Pelletier, E.; lartiges, B. S.; d'Espinose de la Caillerie, J.-B.; Briois, V. *J. Am. Chem. Soc.* **2000**, *122*, 6048.
(26) Chemseddine, A.; Moritz, T. *Eur. J. Inorg. Chem.* **1999**, *2*, 235.
(27) Turillas, X.; Barnes, P.; Dent, A. J.; Jones, S. L.; Norman, C. J. *J. Mater. Chem.* **1993**, *3*, 583.
(28) Michalowicz, A. In *Logiciels pour la Chimie*; Société Francaise de Chimie: Paris, 1991, p 102.
(29) Teo, B. K. In *Inorganic Chemistry Concepts*; Springer-Verlag: Berlin, 1986.
(30) Rehr, J. J.; Albers, R. C. *Phys. Rev. Lett.* **1990**, *41(12)*, 8139.
(31) Zabinsky, S. I.; Rehr, J. J.; Ankudinov, A.; Albers, R. C.; Eller, M. J. *Phys. Rev. B.* **1995**, *52*, 2995.
(32) Chiavacci, L. A.; Pulcinelli, S. H.; Santilli, C. V.; Briois, V. *Chem. Mater.* **1998**, *10*, 986.
(33) Clegg, W. *Acta Crystallogr.* **198**, *43*, 789.
(34) Hazenn, R. M.; Finger, L. W. *AMMIA* **1979**, *64*, 196.
(35) Rose, J. *IFP internal report* **1999**, p 65.
(36) Jaguar 4.1, *Schrödinger, Inc*, Portland, OR, 1991-2000.
(37) Becke, A. D. J. *Chem. Phys.* **1993**, *98*, 5648.
(38) Lee, C.; Yang, W.; Parr, R. G. *Phys. Rev. B* **1988**, *37*, 785.
(39) Hay, P. J.; Wadt, W. R. J. *Chem. Phys.* **1985**, *82*, 270.
(40) Sanchez, C.; In, M. *J. Non−Cryst. Sol.* **1992**, *147 & 148*, 1.
(41) Vaartstra, B. A.; Huffman, J. C.; Gradeff, P. S.; Hubert-Pfalzgraf, L. G.; Daran, J.-C.; Parraud, S.; Yunlu, K.; Caulton, K. G. *Inorg. Chem.* **1990**, *29*, 3126.
(42) Teufer, G. *Acta Crystallogr.* **1962**, *15*, 1187.
(43) De-Bruin, T.; Brosseau, S.; Krokidis, X.; Rose, J.; Toulhoat, H.; Chauveteau, G.; Tabary, R. *J. Phys. Chem. A*, in preparation.
(44) Boyle, T. J.; Schwartz, R. W.; Doedens, R. J.; Ziller, J. W. *Inorg. Chem.* **1995**, *34*, 1110.